DOI:10.1021/ic8017776

Inorganic Chemistry
Article

Hybrid Materials of Lanthanide Centers/Functionalized 2-Thenoyltrifluoroacetone/Silicon−Oxygen Network/Polymeric Chain: Coordination Bonded Assembly, Physical Characterization, and Photoluminescence

Xiao-Fei Qiao and Bing Yan*

Department of Chemistry, Tongji University, Siping Road 1239 Shanghai 200092, China

Received September 17, 2008

2-Thenoyltrifluoroacetone (TTA) was grafted onto the coupling agent 3-(triethoxysilyl)-propyl isocyanate (TEPIC) through a hydrogen transfer addition reaction to construct the multifunctional bridge precursor. Other kinds of polymeric precursors (PVPD, PMAA, and PVPDMAA) were synthesized through the addition polymerization reactions using the monomer 4-vinylpyridine and methacrylic acid as the raw materials. The lanthanide compound was then assembled by the coordination effect between precursors and europium ions with the carbonyl, carboxyl groups, or nitrogen atoms. At last, we have utilized the first precursor hydrolyzed with the tetraethoxysilane (TEOS) via the sol−gel copolycondensation process to obtain three kinds of final hybrid polymers. The photoluminescence and microstructural, thermal, and mechanical properties were characterized and the results reveal that the hybrid materials imbedded into the single polymer (PVPD and PMAA) show more efficient intramolecular energy transfer between the europium ion and the modified ligand TTA-Si, bringing the excellent characteristic emission of europium ion. The different configuration of the polymeric precursor introduces a vital different appearance in the microstructure, and the hybrid material with PVPD shows the highest luminescence quantum efficiency and longest lifetime.

1. Introduction

Lanthanide ions (Ln) have been well-known as important components in luminescent materials, for they have sharp and intense emission bands based on f−f electronic transitions and a wide range of lifetimes that are suitable for various applications. The relatively luminescent material could be excited under suitable conditions because the ligands in the rare earth compound have absorbed the light energy and transferred it to the rare earth ions.[1−6] A lot of reports have focused on the luminescence and intramolecular energy transfer in the rare earth complexes, especially with the ligands β-diketones, aromatic carboxylic acids, and heterocyclic ligands, which could protect center ions from quenching effect aroused by vibrational coupling of the hydroxyl groups, increase the light absorption cross section, exhibit narrow characteristic emissions [7−12] and show an appropriate energy level match and energy transfer system (antenna effect).[13−15] Because the absorption coefficients of organic ligands are many orders of magnitude as large as the intrinsic low molar absorption coefficients of trivalent lanthanide ions,[16] the Eu^{3+} complexes especially containing β-diketone ligand show outstanding sharp emission peaks and high quantum efficiency[17,18] and offer several advantages and potential applications to design efficient light-conversion

*To whom the correspondence should be addressed. E-mail: byan@tongji.edu.cn.. Fax: 86-21-65982287. Phone: 86-21-65984663.

(1) Sabbatini, N.; Guardigli, M.; Lehn, J. M. *Coord. Chem. Rev.* **1993**, *123*, 201.
(2) Elbanowski, M.; Makowska, B. *J. Photochem. Photobiol.* **1996**, *99*, 85.
(3) Weissman, S. I. *J. Chem. Phys.* **1942**, *10*, 214.
(4) Melby, L. R.; Rose, N. J.; Abramson, E.; Caris, J. C. *J. Am. Chem. Soc.* **1964**, *86*, 5117.
(5) Binnemans, K.; Lenaerts, P.; Driesen, K.; Gorller-Walrand, C. *J. Mater. Chem.* **2004**, *14*, 191.
(6) Carlos, L. D.; Sa Ferreira, R. A.; Rainho, J. P.; Bermudez, V. D. *Adv. Funct. Mater.* **2002**, *12*, 819.
(7) Matthews, L. R.; Knobbe, E. T. *Chem. Mater.* **1993**, *5*, 1697.
(8) Casalboni, S. R.; Prospositio, P. *Appl. Phys. Lett.* **1997**, *30*, 2969.
(9) Lebeau, B.; Fowler, C. E.; Hall, S. R. *J. Mater. Chem.* **1999**, *9*, 2279.
(10) Tanner, P. A.; Yan, B.; Zhang, H. J. *J. Mater. Sci.* **2000**, *35*, 4325.
(11) Zhang, H. J.; Fu, L. S.; Wang, S. B.; Meng, Q. G.; Yang, K. Y.; Ni, J. Z. *Mater. Lett.* **1999**, *38*, 260.
(12) Yan, B.; Zhang, H. J.; Wang, S. B.; Ni, J. Z. *Mater. Chem. Phys.* **1997**, *51*, 92.
(13) Bekiari, V.; Lianos, P. *Adv. Mater.* **1998**, *10*, 1455.
(14) Driesen, K.; Deun, R. V.; Gorller-Walrand, C.; Binnemans, K. *Chem. Mater.* **2004**, *16*, 1531.
(15) Braga, S. S.; Sa' Ferreira, R. A.; Gonvalves, I. S.; Pillinger, M.; Rocha, J.; Teixeira-Dias, J. J. C; Carlos, L. D. *J. Phys. Chem. B* **2002**, *106*, 11430.
(16) Klink, S. I.; Grave, L.; Reinhoudt, D. N.; van Veggel, F. C. J. M.; Werts, M. H. V.; Geurts, F. A. J.; Hofstraat, J. W. *J. Phys. Chem. A* **2000**, *104*, 5457.
(17) Robinson, M. R.; O'Regan, M. B.; Bazan, G. C. *Chem. Commun.* **2000**, 1645.
(18) Carlos, L. D.; de Mello Donega, C.; Albuquerque, R. Q.; Alves, S.Jr; Menezes, J. F. S.; Malta, O. L. *Mol. Phys.* **2003**, *101*, 1037.

Published on Web 4/17/2009

molecular devices (LCMD).[19−21] However, as tunable solid-state laser or phosphor devices, the lanthanide complexes without any modification have not been qualified because of their poor stability and mechanical strength under high temperature, high pressure, or moist conditions. So the lanthanide complexes should commonly be incorporated into inorganic matrices by the low-temperature soft-chemistry sol−gel method.

Inorganic−organic hybrid materials have attracted considerable attention with the expansion of soft inorganic chemistry processes and provided a wealth of opportunities for combination of organic and inorganic networks to exhibit their extraordinary properties such as luminescent systems in lighting displays, optical amplifiers, and lasers.[22,23] According to the interaction between the organic and inorganic components or phases, these hybrid materials can be divided into two major classes. One is so-called physically mixed by weak interactions (hydrogen bonding, van der Waals force, or weak static effects) between the organic and inorganic phases; the other is chemically bonded by powerful covalent bonds.[24−30] In the first class, although the metal complex, especially lanthanide organic complexes that have been doped into a silica matrix, have shown superior emission intensities and organic components are considered to be efficient sensitizers for the rare earth ions, this kind of material cannot solve the problems of the quenching effect of luminescent centers, inhomogeneous dispersion of two phases, or leaching of the photoactive molecules with a low concentration of the complex. Moreover, because the latter class hybrid material belongs to the molecular-based composite material with excellent chemical stability and a monophasic appearance even with a high concentration of lanthanide complexes,[31−44] we can tailor the multifunctional advanced materials for different demands in physiology, biochemistry, and photochemistry areas through the combination of the different components with chemical bonds.[45] Franville A. C. and co-workers have concentrated on complexes of rare earth−pyridine−dicarboxylic acid or their derivatives, and the molecular-based dicarboxylic acid derivative materials have exhibited strong emissions.[36] Zhang H. J. et al. started to modify 1,10-phenanthroline and dipyridine in order to prepare the determined molecular-level hybrid materials.[31] However, the above rare earth hybrid complexes merely contain an organic ligand component and an inorganic silicon−oxygen network component, and the polymerization reactions occur just between silicanes and water molecules (so-called inorganic polymerization) to form an Si−O−Si network in a sol−gel procedure.

Compared to this kind of rare earth hybrid with Si−O polymeric networks, fewer reports on molecular rare earth hybrid materials fabricated with organic network and inorganic polymers have been published,[46−50] possibly because suitable polymers or monomers are hard to select. Recently, more professional investigations have been altered to focus on the rare earth hybrid materials concerning inorganic and organic polymerization reactions or imbedding certain polymers containing long carbon chains by covalent bonds. It has been proven that hybrid materials with inorganic networks and organic polymers with high molecular weight have excellent effective properties, because each dispersed molecule is a luminescence unit so that the transparency, dimension, and concentration of dispersed rare earth composite molecules and the interfacial interaction between the rare earth organic complex and the polymer matrix are primary factors to influence the final luminescence properties of the materials. Ultimately, the homogeneous dispersion of smaller particles leads to a higher transparency of the composite and the larger interfacial region between the complex particles and the polymer matrix at a larger scale, which would improve the efficiency of excitation process. The larger interfacial region and the stronger interaction between the rare earth complex and polymer matrix might accelerate the energy transfer mechanism so as to facilitate the fluorescence emission and enhance the luminescence intensities.

Our team has dedicated ourselves in the design of the rare earth hybrid materials with either inorganic silicon−oxygen networks or organic polymeric long carbon chains for several years,[51−55] and in recent years, we put forward a novel path to assemble the hybrid materials containing inorganic and organic networks simultaneously.[56] In view of the mechanically stable, easily processed, and conveniently storied properties of the polymer, we have synthesized the polymer (PVPD, PMAA, and PVPDMAA) to construct the polymeric chains (C−C); subsequently, we have modified

(19) Lehn, J. M. *Angew. Chem., Int. Ed.* **1990**, *29*, 1304.
(20) Hu, W.; Matsumura, M.; Wang, M.; Jin, L. *Appl. Phys. Lett.* **2000**, *77*, 26.
(21) Zheng, Y. X.; Fu, L. S.; Zhou, Y. H.; Yu, J. B.; Yu, Y. N.; Wang, S. B.; Zhang, H. J. *J. Mater. Chem.* **2002**, *12*, 919.
(22) Molina, C.; Dahmouche, K.; Santilli, C. V.; Craievich, A. F.; Ribeiro, S. J. L. *Chem. Mater.* **2001**, *13*, 2818.
(23) Suratwala, T.; Gardlund, Z.; Davidson, K.; Uhlmann, D. R. *Chem. Mater.* **1998**, *10*, 190.
(24) Sanchez, C.; Ribot, F. *New J. Chem.* **1994**, *18*, 1007.
(25) Koslova, N. I.; Viana, B.; Sanchez, C. *J. Mater. Chem.* **1993**, *3*, 111.
(26) Harreld, J. H.; Esaki, A.; Stucky, G. D. *Chem .Mater.* **2003**, *15*, 3481.
(27) Minoofar, P. N.; Hernandez, R.; Chia, S.; Dunn, B.; Zink, J. I.; Franville, A. C. *J. Am. Chem. Soc.* **2002**, *124*, 14388.
(28) Choi, J.; Tamaki, R.; Kim, S. G.; Laine, R. M. *Chem .Mater.* **2003**, *15*, 3365.
(29) Franville, A. C.; Zambon, D.; Mahiou, R.; Chou, S.; Troin, Y.; Cousseins, J. C. *J. Alloys Compd.* **1998**, *275−277*, 831.
(30) Franville, A. C.; Mahiou, R.; Zambon, D.; Cousseins, J. C. *Solid State Sci.* **2001**, *3*, 211.
(31) Li, H. R.; Lin, J.; Zhang, H. J.; Fu, L. S. *Chem. Mater.* **2002**, *14*, 3651.
(32) Li, H. R.; Lin, J.; Zhang, H. J.; Fu, L. S. *Chem. Commun.* **2001**, 1212.
(33) Yan, B.; Wang, F. F. *J. Organomet. Chem.* **2007**, *692*, 2395.
(34) Yan, B.; Qiao, X. F. *Photochem. Photobiol.* **2007**, *83*, 971.
(35) Qiao, X. F.; Yan, B. *J. Photochem. Photobiol., A* **2008**, *199*, 188.
(36) Franville, A. C.; Zambon, D.; Mahiou, R. *Chem. Mater.* **2000**, *12*, 428.
(37) Wang, Q. M.; Yan, B. *J. Mater. Chem.* **2004**, *14*, 2450.
(38) Wang, Q. M.; Yan, B. *J. Mater. Res.* **2005**, *20*, 592.
(39) Wang, Q. M.; Yan, B. *Cryst. Growth Des.* **2005**, *5*, 497.
(40) Yan, B.; Ma, D. J. *J. Solid State Chem.* **2006**, *179*, 2059.
(41) Sui, Y. L.; Yan, B. *J. Photochem. Photobiol., A* **2006**, *182*, 1.
(42) Carlos, L. D.; Sa'Ferreira, R. A.; Pereira, R. N.; Assuncao, M.; de Zea Bermudez, V. *J. Phys. Chem. B* **2004**, *108*, 14924.
(43) Goncalves, M. C.; de Zea Bermudez, V.; Sa' Ferreira, R. A.; Carlos, L. D.; Ostroviskii, D.; Rocha, J. *Chem. Mater.* **2004**, *16*, 2530.
(44) Lenaerts, P.; Storms, A.; Mullens, J.; Dhaen, J.; Gorller-Walrand, C.; Binnemans, K.; Driesen, K. *Chem. Mater.* **2005**, *17*, 5194.
(45) Kawa, M.; Frechet, J. M. *J. Chem. Mater.* **1998**, *10*, 286.
(46) Iwamura, R.; Higashiyama, N.; Takemura, K.; Tsutsumi, S.; Kimura, K.; Adachi, G. *Chem. Lett.* **1994**, 1131.
(47) Chen, H. Y.; Archer, R. D. *Macromolecules* **1996**, *29*, 1957.
(48) Bekiari, V.; Pistolis, G.; Lianos, P. *Chem. Mater.* **1999**, *11*, 3189.
(49) Wang, L. H.; Wang, W.; Zhang, W. G.; Kang, E. T.; Huang, W. *Chem. Mater.* **2000**, *12*, 2212.
(50) Wang, Q. M.; Yan, B. *J. Photochem. Photobiol., A* **2006**, *177*, 1.
(51) Wang, Q. M.; Yan, B. *J. Photochem. Photobiol., A* **2006**, *178*, 70.
(52) Wang, Q. M.; Yan, B. *J. Organomet. Chem.* **2006**, *691*, 540.
(53) Wang, Q. M.; Yan, B. *J. Organomet. Chem.* **2006**, *691*, 3567.
(54) Wang, Q. M.; Yan, B. *Inorg. Chem. Commun.* **2004**, *7*, 1124.
(55) Qiao, X. F.; Yan, B. *J. Phys. Chem. B* **2008**, *112*, 14742.
(56) Yan, B.; Qiao, X. F. *J. Phys. Chem. B* **2007**, *111*, 12362.

β-diketones TTA with the electrophilic reagent to obtain the functional covalently bonded precursor (TTA-Si) and obtained the final hybrid polymers with a combination of the europium−β-diketones compound and silicon−oxygen networks after the coordinating, hydrolysis, and cross-linking condensation reactions. Our target is to use the polymer as the controller and sensitizer to obtain materials with the optical quality deriving from the intramolecular energy transfer system. Besides, we use the polymer to control the microstructure of the materials through the self-assembly mechanism confirmed by unique microstructure and the photoluminescence properties discussed in the paper.

2. Experimental Section

2.1. Chemicals. Europium nitrate was obtained by dissolving Eu_2O_3 in concentrated nitric acid. Tetraethoxysilane (TEOS, Aldrich) was distilled and stored under a nitrogen atmosphere. 3-(Triethoxysilyl)-propyl isocyanate (TEPIC) and 4-vinylpyridine were purchased from the Lancaster Company, 2-thenoyltrifluoroacetone (TTA) and methacrylic acid (MAA) was purchased from Shanghai chemical plant, and the solvent tetrahydrofuran (THF) was used after desiccation with anhydrous calcium chloride. All other reagents were analytically pure.

2.2. Synthetic Procedures. 2.2.1. Synthesis of Polymer Precursors (PVPD, PMAA, and PVPDMAA). 4-Vinylpyridine (2 mmol, 3 mL) for PVPD, methacrylic acid (2 mmol, 4 mL) for PMAA, and 4-vinylpyridine (2 mmol, 3 mL) and methacrylic acid (2 mmol, 4 mL) for PVPDMAA were dissolved in a small quantity of tetrahydrofuran (THF) solution (6 mL) with initiator (BPO, benzoyl peroxide), and the polymers were then constructed through addition polymerization under argon atmosphere purging. The reaction temperature was maintained at 50 °C and the reaction times are about 4 h for PMAA to obtain the colorless viscid liquid and 6 h for PVPD and PVPDMAA to obtain the brown viscid liquid. The obtained materials were concentrated under room temperature to remove the solvent THF using a rotary vacuum evaporator, and the viscous liquid was obtained (PVPD $[C_7H_7N]_n$, PMAA $[C_4H_6O_2]_n$, PVPDMAA $[C_{11}H_{13}O_2N]_n$ (see Figure 1). The weight average molecular weight and molecular distribution are 7.2×10^3 and 1.58 for PVPD, 1.34×10^4 and 1.45 for PMAA, and 9.1×10^3 and 1.51 for PVPDMAA, respectively. The three kinds of viscid liquid were dissolved in the solvent *N*,*N*-dimethyl formamide (DMF) for the coordination reaction with rare earth ions.

2.2.2. Synthesis of the Cross-Linking Precursors Containing Si−O Chemical Bonds (TTA-Si). 2-Thenoyltrifluoroacetone (TTA) (1 mmol, 0.222 g) was first dissolved in the solvent dehydrate tetrahydrofuran (THF) (20 mL), and NaH (2 mmol, 0.048 g) was then added into the solution with stirring at the temperature of 65 °C. Two hours later, 2.0 mmol (0.495 g) of 3-(triethoxysilyl)-propyl-isocyanate (TEPIC) was added into the refluxed solution. The mixture was heated at 65 °C in a covered flask for approximately 12 h at the nitrogen atmosphere. The brown liquid sample was then dissolved in absolute ethanol, and 20 mL of hexane was added to the solution to purify the liquid sample. Subsequently, the solution was washed and extracted. The above procedures involving dissolution and extraction were repeated three times. At last, the pure brown viscous liquid TTA-Si was obtained and preserved in a vacuum with the yield 75% (see Figure 2). The ^{1}HNMR data are as follows: ($C_{28}H_{47}O_{10}F_3N_2Si_2S$) δ 0.50 (4H, t), 1.13 (18H, t), 1.41 (4H, m), 2.95 (4H, t), 3.73 (12H, m), 5.90 (2H, t), 7.06 (1H, d), 7.53 (1H, d), 7.65 (1H, d). The ^{13}CNMR data are as follows: δ 5.21 (CH_2Si), 7.38 ($CH_2CH_2CH_2$), 18.22 (CH_3CH_2O), 23.75 (C $(C{=}O)_4$), 42.26 (NCH_2CH_2), 57.81 (CH_3CH_2O), 86.88

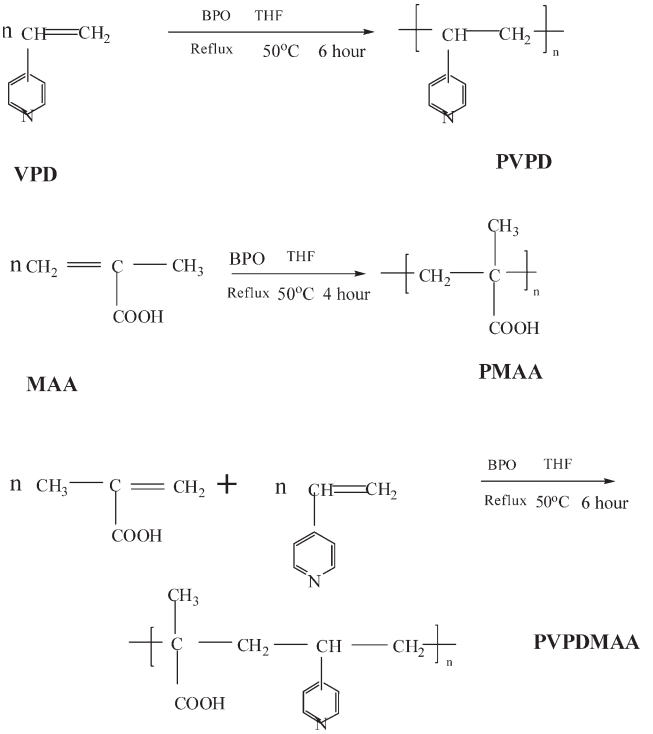

Figure 1. Scheme of synthesis processes of the polymeric precursors (PVPD, PMAA, and PVPDMAA).

(CF_3), 120.83 (CH = CHS), 124.43 ($CH{=}CHCH{=}C$), 126.78 ($CHCH{=}CSC{=}O$), 127.92 ($CH{=}CSC{=}O$),δ149.36 ($CC{=}ONH$), 158.37 ($SCC{=}OC$), 179.15 ($CF_3C{=}O$). Therefore, we could infer that the precursor TTA-Si has been synthesized successfully proved by the data. The precursor TTA-Si was dissolved in the solvent *N*,*N*-dimethyl formamide (DMF) for the coordination reaction with rare earth ions.

2.2.3. Synthesis of Three Kinds of the Hybrid Materials Imbedded into Si−O Networks and Organic Carbon Chains through Chemical Bonds (TTA−Si−Eu−PVPD/PMAA/PVPDMAA). A stoichiometric amount of $Eu(NO_3)_3 \cdot 6H_2O$ (0.3 mmol, 0.136 g) was added dropwise into the DMF solution of precursors TTA-Si and PVPD (PMAA and PVPDMAA) while stirring. After 6 h, stoichiometric amounts of TEOS and H_2O were added into the mixed solution after the coordination reaction has completed between precursors TTA-Si and PVPD (PMAA and PVPDMAA) and europium ions, which accompanied the addition of one drop of dilute hydrochloric acid to promote hydrolysis. The $RE(NO_3)_3 \cdot 6H_2O$:TTA-Si:PVPD (PMAA and PVPDMAA):TEOS:H_2O molar ratio was 1:3:1:6:24. (the polymer obtained in the above process, TEOS 0.45 mL, 0.833 g, and H_2O 0.288 g). After the treatment of hydrolysis, an appropriate amount of hexamethylene-tetramine was added to adjust the pH to 6−7. The mixture was agitated magnetically to achieve a single phase in a covered Teflon beaker and was then aged at 70 °C until the onset of gelation in 5−7 days. The gels were collected as monolithic bulks and ground into powdered material for the photophysical studies (see Figure 2)

2.3. Physical Measurement. ^{1}H NMR and ^{13}C NMR spectra were recorded in DMSO on a BRUKER AVANCE-500 spectrometer with tetramethylsilane (TMS) as inter-reference. The molecular weight and weight distribution were determined through gel-permeation chromatography (GPC) by WATERS 1515 with polystyrene as standard sample. FTIR spectra were measured within the 4000−400 cm^{-1} region on an infrared spectrophotometer with the KBr pellet technique. The ultraviolet absorption spectra (5×10^{-4} mol L^{-1} DMF solution)

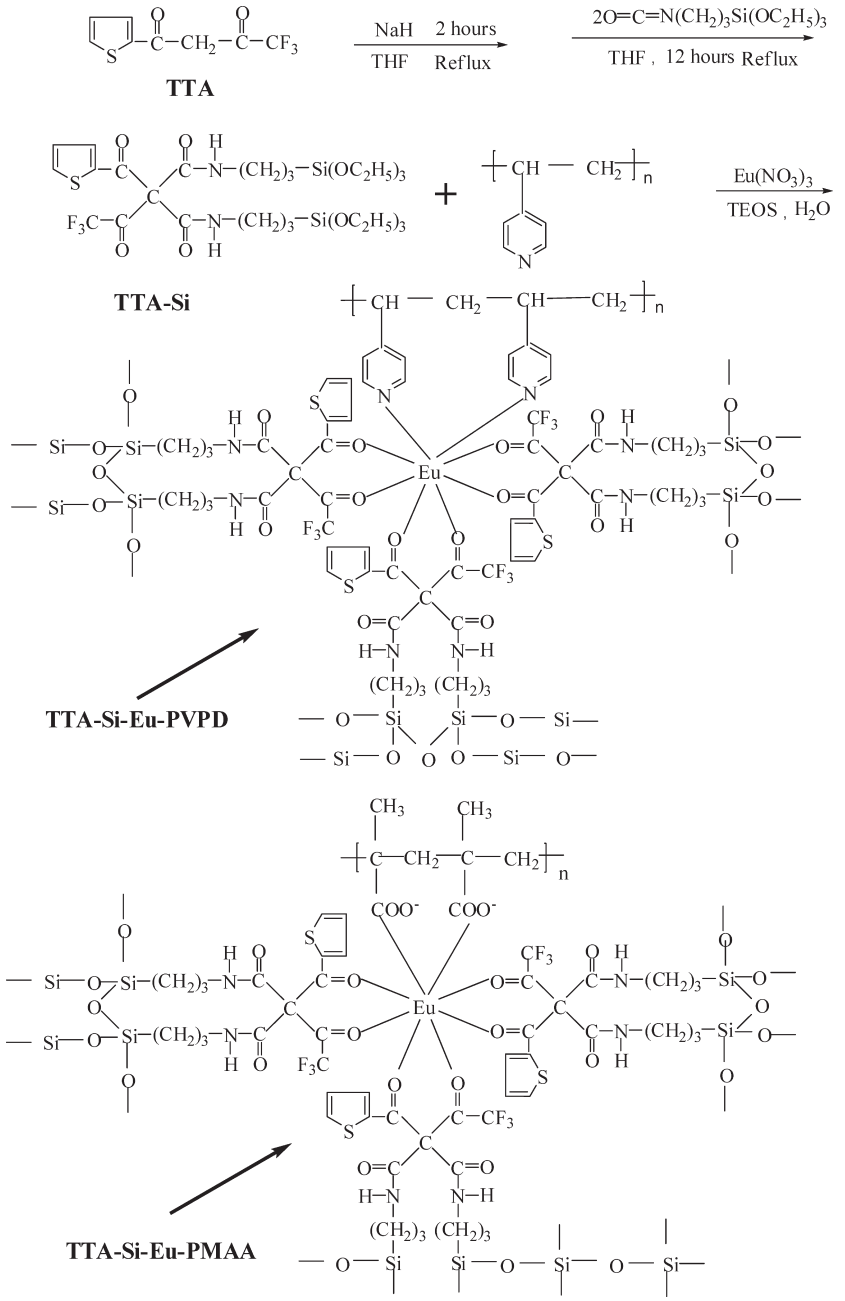

Figure 2. Scheme of synthesis processes of the precursor (TTA-Si) and hybrid polymeric materials TTA−Si−Eu−PVPD and TTA−Si−Eu−PMAA.

and the ultraviolet−visible diffuse reflection spectra of the powder samples were recorded by an Agilent 8453 spectrophotometer and a BWS003 spectrophotometer, respectively. The X-ray diffraction (XRD) measurements of the powdered sample were carried out by a BRUKER D8 diffractometer (40 mA, 40 kV) using monochromated Cu Ka1 radiation (k = 1.54 Å) over the 10−70° 2θ range. Thermogravimetry (TG) data were obtained on Netzsch, model STA 409C, in the following conditions: oxygen air atmosphere, heating/cooling rate of 10 °C/min, 18.78 mg of powder, and crucibles of Al_2O_3. Scanning electronic microstructure (SEM) was measured on a Philip XL30. The fluorescence excitation and emission spectra were obtained on a RF-5301 spectrophotometer, excitation and emission slit width = 3 nm. Luminescence lifetime measurements were carried out on an Edinburgh FLS920 phosphorimeter using a 450 W xenon lamp as excitation source. All above measurements were completed at room temperature.

3. Results and Discussion

3.1. Spectra Analysis for the Raw Materials, The Precursors and the Hybrid Materials. 3.1.1 NMR Data Analysis. We have tested the ^{1}H and ^{13}C NMR of the precursor TTA-Si and represented the data in the synthesis procedure above and the original figures in the Supporting Information. It is seen from Figure S2 that the peak (f) located at 5.90 ppm assigned to the characteristic signal of the group −NH− has not been observed in Figure S4 (the data of the raw material TEPIC), and peak (a) at 6.91 ppm in Figure S3 aroused by the group of methylene of the raw material TTA disappeared in Figure S2, because the group −C−NH− was formed through the hydrogen transfer addition reaction between TTA and TEPIC. Moreover, every peak has shifted slightly in Figure S2 compared with that in Figures S3

and S4, especially the perk (d) located at 3.30 ppm in Figure S4, with the largest shift to 2.95 ppm in Figure S2 as the result of the most primary influence of the hydrogen transfer addition reaction on the group methylene nearest to the nitrogen atom. The integral values of all the peaks are proportional to the amount of protons in TTA-Si. According to the NMR data, we could deduce that the ligand TTA have been grafted onto TEPIC and the precursor TTA-Si has been synthesized. However, it is very difficult to isolate the TTA-Si from the raw materials (TTA and TEPIC) or the solvent (THF) completely, because the precursor we've obtained is a viscous liquid and when we added the solvent hexane into the precursor TTA-Si dissolved in ethanol for purification, some oil components were still suspended in the solution so that we could not obtain the TTA-Si with 100% purity thrugh the extraction procedure. Comparing the ^{1}H NMR figure of TTA-Si to the figures of TTA and TEPIC, it is indicated that the impurity peaks 1, 2, 6, and 7 in TTA-Si have derived from the impurity peaks of the unreacted raw material TTA, the peaks 3, 4, and 5 are also assigned to the impurity peaks of the unreacted raw materials TEPIC, all of which have been marked in the figures.

3.1.2. FT-IR Spectra. The FTIR spectra of the free β-diketone ligand (TTA), the precursor (TTA-Si) and the hybrid polymeric material are shown in Figure 3. In view of the free ligand TTA (A), it can be observed that the stretching vibration of $-CH_2-$ at 3119 cm^{-1} was substituted by a strong broadband located at 2977, 2922, and 2886 cm^{-1} in B that originates from the three methylene groups of 3-(triethoxysilyl)-propyl isocyanate (TEPIC). In addition, the spectra of TTA-Si are dominated by stretching vibration absorption bands ν (C−Si, 1277 cm^{-1}) and ν (Si−O, 1079 cm^{-1}), characteristic of trialkoxylsilyl functional group, and the band centered at 3378 cm^{-1} corresponds to the stretching vibration of grafted −NH− group in B. The bending vibration (δ_{NH}, 1410 cm^{-1}) further proves the formation of amide groups. New peaks at 1626 and 1528 cm^{-1} are due to the absorption of −CONH− group deriving from the cross-linking reagent TEPIC, proving that 3-(triethoxysilyl)-propyl isocyanate was successfully grafted onto β-diketone ligand. The spectra of the hybrid polymeric material (C) indicates that the formation of the Si−O−Si framework is evidenced by the broad bands located at about 1027−1134 cm^{-1} (ν_{as}, Si−O), 823 cm^{-1} (ν_s, Si−O), and 463 cm^{-1} (δ, Si−O−Si), which attributes to the success of hydrolysis and copolycondensation reactions. (ν represents stretching, δ in plane bending, s symmetric, and as asymmetric vibrations) Furthermore, the peaks at 1662 and 1608 cm^{-1} originating from the −CONH− group of TTA-Si, can also be observed in C, which is consistent with the fact that the carbonyl groups of the precursor remain invariability after hydrolysis and condensation reactions, because the two carbonyl groups of β-diketones coordinated to the rare earth ions, not the carbonyl groups of the TEPIC.[35] Moreover, the strong sharp peak at about 1580 cm^{-1} in A, assigned to the existence of the carbonyl groups of the β-diketones, disappeared in C, also indicating that the carbonyl groups of the ligand β-diketones successfully coordinated to the rare earth ions, which presents the same conclusion with the above.

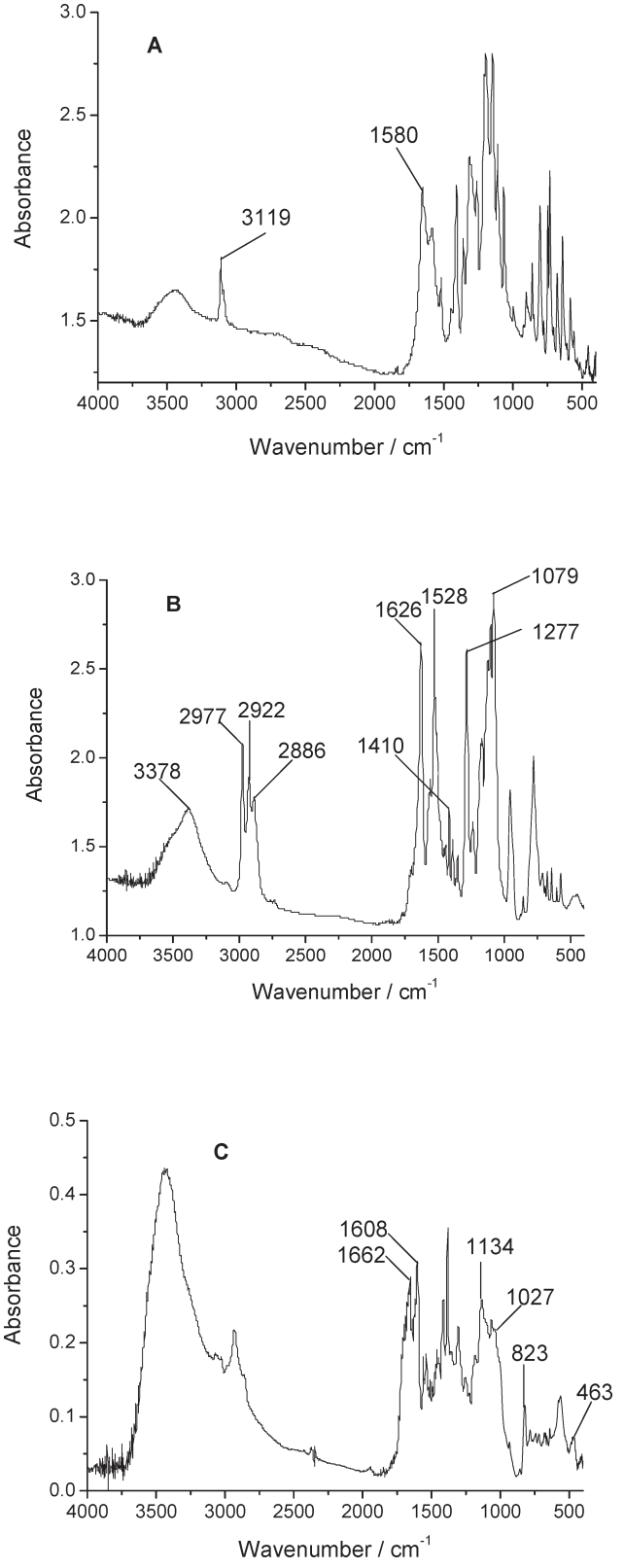

Figure 3. Fourier transform infrared spectra of the (A) free ligand TTA, (B) precursor TTA-Si, and (C) the hybrid material TTA−Si−Eu−PVPD.

3.1.3. Ultraviolet Absorption Spectra. Figure 4 exhibits the ultraviolet absorption spectra of TTA (A) and TTA-Si (B). From the spectra, it can be observed that an

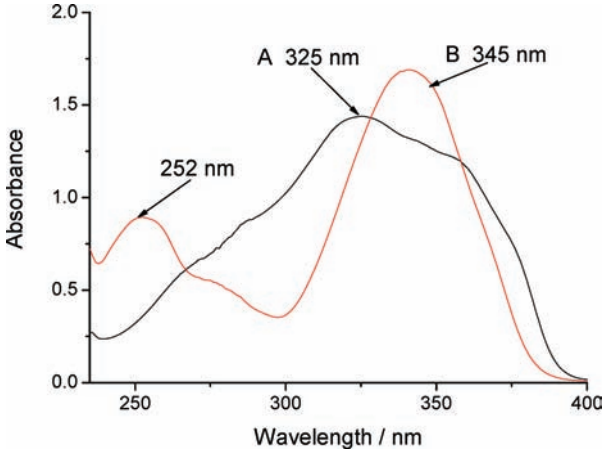

Figure 4. Ultraviolet absorption spectra of (A) the free ligand TTA and (B) the precursor TTA-Si.

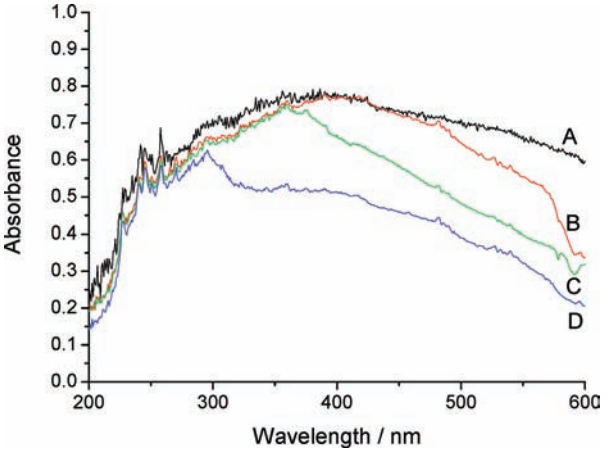

Figure 5. Ultraviolet−visible diffuse reflection absorption spectra of the hybrid polymeric materials and the ligand: (A) TTA−Si−Eu-PVPD, (B) TTA−Si−Eu−PMAA, (C) TTA−Si−Eu−PVPDMAA, and (D) TTA.

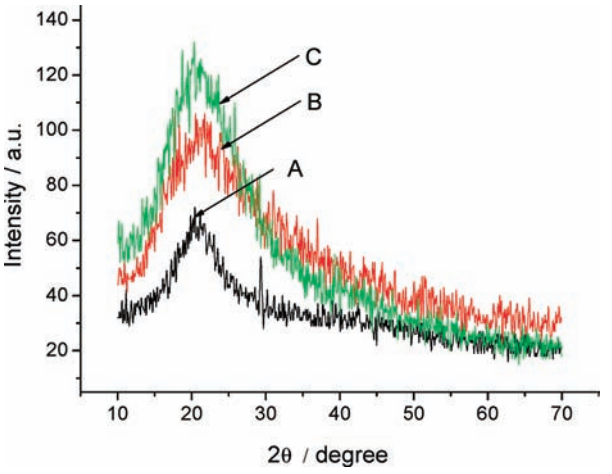

Figure 6. X-ray diffraction patterns for hybrid materials: (A) TTA−Si−Eu−PVPD, (B) TTA−Si−Eu−PMAA, and (C) TTA−Si−Eu−PVPDMAA.

obvious red shift (about 20 nm) of the major $\pi-\pi^*$ electronic transitions A→B (from 325 to 345 nm) indicate the electron distribution of the modified TTA-Si has been changed compared to free ligand TTA and that new electron conjugate construction of the new material has been produced because of the introduction of the carbonyl group. The synthesis for the precursor TTA-Si has increased the wavelength of the TTA-Si up to 20 nm, and the energy difference of the electronic orbits has decreased to bring more conjugated properties, so it is easier for electrons transition after the grafted procedure. Therefore, we could deduce that the 3-(triethoxysilyl)-propyl isocyanate has been grafted onto the ligand β-diketones (TTA) successfully.

3.1.4. Ultraviolet−Visible Diffuse Reflection Absorption Spectra. The ultraviolet−visible diffuse reflection absorption spectra of the hybrid materials are given in Figure 5. The three lines denote the rare earth hybrid polymeric materials (A for TTA−Si−Eu-PVPD, B for TTA−Si−Eu-PMAA, C for TTA−Si−Eu-PVPDMAA and D for TTA). It is observed that all the wide bands of the A, B and C are located at about 300−420 nm, which partially overlaps with the fluorescence excitation spectra (wide bands at 320−370 nm in Figure 9a) and also with the absorption spectra of the free ligand (TTA) at 275−394 nm. Following Dexter's exchange energy transfer theory: [57] the luminescence intensity of hybrid material depends on the matching degree between the ligand's triplet state energy and lanthanide ion's excited-state energy, it can be primarily predicted that the energy level difference between TTA and Eu^{3+} is suited so that the organic ligand can absorb abundant energy in ultravisible extent to transfer energy to the corresponding hybrid material. Then the final hybrid materials can be expected to possess excellent luminescence properties after intramolecular energy transfer process has completed, which is proved by the fluorescence spectra in Figure 9. And it is observed the peak shapes of the TTA−Si−Eu-PVPD and TTA−Si−Eu-PMAA have some resemblance, a little different from TTA−Si−Eu-PVPDMAA. One possibility we presumed is that the single polymer PVPD and PMAA were been synthesized through the addition polymerization reaction using the 4-vinylpyridine and the methacrylic acid as the single monomer, respectively, while the PVPDMAA is a copolymer through the copolymerization reaction between two kinds of the monomers. Therefore the polymer PVPDMAA has the pyridine ring and carboxyl groups simultaneously in such a small space, which has brought huge steric hindrance effect in the coordination process.

3.1.5. Powder XRD Spectra. The room-temperature X-ray diffraction patterns from 10 to 70 ° of the hybrid materials are shown in Figure 6, exhibiting that the obtained hybrid materials are amorphous in a wide region. The broad peaks center on about 20.35°, 4.362 Å for A, 21.41°, 4.148 Å for B, and 20.55°, 4.32 Å for C, because of the amorphous siliceous backbone of the hybrids.[58] The absence of any crystalline regions in these materials correlates with the presence of inorganic networks. Moreover, because the siliceous backbones belong to the inorganic region and possess less orderliness, the hybrid materials still hold a disordered sequence even after the polymer has been imbedded; the existence of polymer did not decrease the overall disorder of the siliceous

(57) Dexter, D. L. *J. Chem. Phys.* **1953**, *21*, 836.

(58) Gao, B. J.; Yang, Y. F.; Cheng, Y.; Shi, D. J. *Spectrosc. Spectra Anal.* **2002**, *22*, 371.

skeleton seen from the data, although polymeric carbons chains of the polymer are essentially regularly ordered.

3.2. Thermogravimetric and Microstructure Properties Analysis for the Hybrid Materials. 3.2.1. Thermogravimetry Trace. Figure 7 shows the thermogravimetry trace (TG) (a) and differential thermogravimetry trace (DTG) (b) of the hybrid polymeric material TTA−Si−Eu−PVPD. Seen from TG curve a, the hybrid material TTA−Si−Eu−PVPD has lost mass (about 14.24%) from 132.5 °C until 245.5 °C. It is deduced that part of the hydrogen atoms have formed vapor with a few oxygen atoms of the hybrid material or from the external oxygen atmosphere; simultaneously, part of the nitrogen atoms have formed nitrogen dioxide in the oxygen atmosphere and actually weigh about 13.32% of the whole molecular weight based on the molecular formula, close to the result shown in the thermogravimetric data. Moreover, according to the molecular formula of the hybrid material TTA−Si−Eu−PVPD, the polymer PVPD occupies about one-fourth (24.24%) of the weight, and the graph shows that there is a mass loss about 25.94% from 330.3 to 414.7 °C. In addition, the hybrid material lost mass at the rapidest speed when the temperature climbed to 376.42 °C, which is observed from the DTG curve with the sharpest peak. The PVPD began to decompose at 330.3 °C; when the temperature reached 414.7 °C, the polymer PVP had departed from the hybrid material completely. Finally, the material TTA−Si−Eu−PVPD retains a mass of about 36.24%, which represents the weight of the Si−O networks and rare earth ions.

3.2.2. Scanning Electron Micrographs. The scanning electron micrographs of the hybrid polymeric materials in Figure 8 demonstrate that the homogeneous, molecular-based materials, which belong to a complicated huge molecular system, were obtained with covalent bonds between the organic β-diketone ligand and the inorganic matrix and the coordinate bonds between organic β-diketone ligand or polymer ligand and rare earth ions. Compared to the hybrid materials with doped lanthanide complexes, which generally experience phase separation phenomena, in this paper, the hybrid material we obtained exhibits the distinct properties together in the monophasic condition deriving from both inorganic and organic phases.[59]

The hybrid material A (TTA−Si−Eu-PVPD) is composed of many regular and uniform dendritic stripes microstructure seen from Figure 8A1, and there are many holes with the same diameter size of about 800 nm around the stripes seen from Figure 8A2. There are two possible reasons for the holes: one is the largely different thermal expansion coefficients between the polymer PVPD and silicane, the other is the evaporation and escape effect of solvent (THF) through the thermal procedure.[60] Therefore, the moiety of polymer PVPD plays an important role in the preparation of hybrid materials. Furthermore, another phenomenon was found in Figure 8B that there exist plenty of tridimensional spheres with the uniform diameter size of about 500 nm distributed regularly on the surface of hybrid material. It is observed that there are

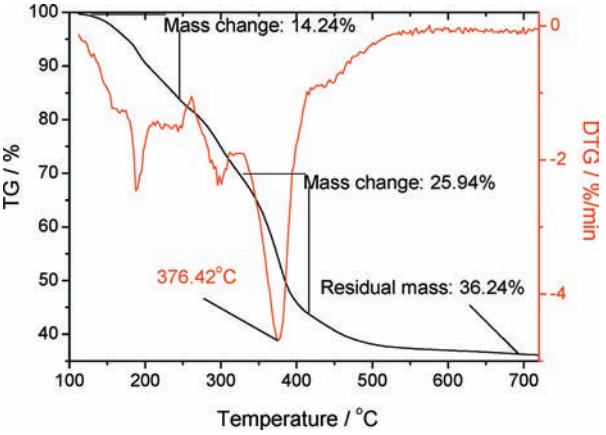

Figure 7. Thermogravimetry trace (TG) and differential thermogravimetry trace (DTG) of the hybrid material TTA−Si−Eu−PVPD.

many uniform trunk stripes with the same size dispersed on the surface of TTA−Si−Eu−PVPDMAA seen from Figure 8C.

The precursor TTA-Si is a derivative precursor from 2-thenoyltrifluoroacetone, which has two carbonyl groups and one trifluoromethyl. Its corresponding rare earth complexes are ready to form two-dimensional layerlike or three-dimensional networklike structure easily while not the polymeric structure; this two-dimensional layerlike structure or three-dimensional networklike structural tendency will compete with the construction of the polymeric network structure of Si−O−Si in the hydrolysis and copolycondensation processes or with the formation of the coordinate bonds between rare earth ions and polymer precursors. Therefore, both of the tendencies have respective influence on the formation of the obtained hybrid polymeric materials, even leading to the final micromorphology seen in Figure 8. Moreover, it is observed that the microstructures of the TTA−Si−Eu−PVPD and TTA−Si−Eu−PVPDMAA are different from that of TTA−Si−Eu−PMAA. One possibility is that the polymer 4-vinylpyridine has the pyridine ring, which has not been changed at all in the polymerization reaction or copolymerization reaction and played an important role in the dimensional conformation in the coordinating and hydrolysis processes. However, the methacrylic acid merely has carbon chains; when the polymerization reaction has occurred, the structure on its own has been changed entirely, chains becoming longer and longer without the existence of primary conformation. Thus, the existence of the pyridine ring has affected the tendency of TTA-Si to form the two-dimensional layerlike or three-dimensional networklike structure, and the tendency to form the striped structure of polymeric networks has occupied the main position in the materials TTA−Si−Eu−PVPD and TTA−Si−Eu−PVPDMAA, whereas the microstructure of TTA−Si−Eu−PMAA merely with the carbon chains is composed by spheres because of the main tendency of the TTA-Si. Another possibility is that the polymer precursor PVPD and PVPDMAA were synthesized through the copolymerization reaction between the 4-vinylpyridine and methacrylic acid to form the longer carbon chains with pyridine rings, bringing more polymeric units in certain limit space. Therefore, the growth of these granules in

(59) Sa Ferreira, R. A.; Carlos, L. D.; Goncalves, R. R.; Ribeiro, S. J. L.; Bermudez, V. D. *Chem. Mater.* **2001**, *13*, 2991.
(60) Yua, Y. Y.; Chen, C. Y.; Chen, W. C. *Polymer* **2003**, *44*, 593.

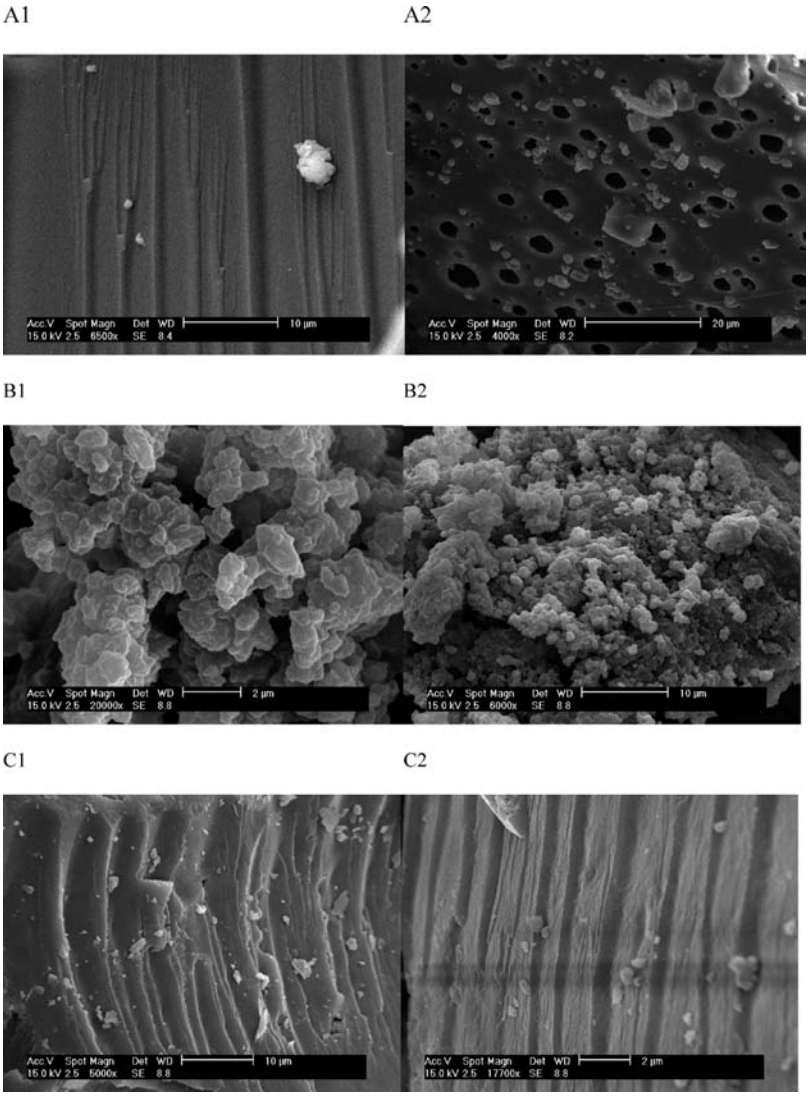

Figure 8. SEM images of the hybrid materials: (A) TTA−Si−Eu-PVPD, (B) TTA−Si−Eu−PMAA, and (C) TTA−Si−Eu−PVPDMAA.

TTA−Si−Eu−PVPD and TTA−Si−Eu−PVPDMAA has been hindered in such crowed circumstance and it is predicted that the different dimensional conformation could have great influence on the microstructure properties of the hybrid polymeric materials.

3.3. Photoluminescence Property Analysis for the Hybrid Materials. 3.3.1. Fluorescent Spectra. Figure 9 shows the excitation (a) and emission (b) spectra of hybrid polymeric materials containing Eu^{3+} covalently bonded into silicon−oxygen networks and carbon chains. The excitation spectra of these materials were all obtained by monitoring the emission wavelength of the Eu^{3+} at 613 nm. For the excitation spectra, three broad absorption peaks are all located at 350 nm, suggesting the characteristic charge transfer between Eu^{3+} and the ligand 2-thenoyltrifluoroacetone (TTA) and the effective absorption of the Eu-TTA system. As a result, in Figure 9b, the emission lines of the three hybrid materials are assigned to the $^5D_0 \rightarrow {}^7F_J$ ($J = 0, 1, 2, 3, 4$) transitions at about 577, 589, 613, 651, and 723 nm for Eu^{3+}. It is noteworthy that seen from the lines of A and B, the ligand emission background completely vanished in the emission spectra under the excitation wavelength at 350 nm, and only the characteristic emissions of Eu ions can be found, whereas as seen from the line of C, the high baseline could correspond to the absorbance of Si−O network. Among these emission peaks of the materials chelating Eu^{3+}, red emission intensities (arbitrary unit, a. u.) of electric dipole transition of $^5D_0 \rightarrow {}^7F_2$ at about 613 nm (611.6 for A, 419.6 for B, and 300.7 for C) are all stronger than the orange emission intensities of magnetic dipole transition of $^5D_0 \rightarrow {}^7F_1$ at about 589 nm (93.9 for A, 60.1 for B, and 240.2 for C, respectively). Because the $^5D_0 \rightarrow {}^7F_2$ transition strongly varies with the local symmetry of Eu^{3+}, while the $^5D_0 \rightarrow {}^7F_1$ transition is independent of the host material, the excitation spectra indicate that the Eu^{3+} site is situated in an environment without inversion symmetry.[41] Therefore, it is indicated that the effective energy transfer took place between the precursors and the chelated rare earth ions. Other factors cannot still be excluded such as relatively rigid structure of silica gel, which limits the vibration of hydroxyl groups in the hybrid materials and prohibits nonradiative transitions. Accordingly, we may expect that through this efficient manner, leaching of the photoactive molecules and clustering of the emitting centers could be avoided, and higher concentration of metal ions will be realized. In Figure 9b, the emission spectra of A and B show some

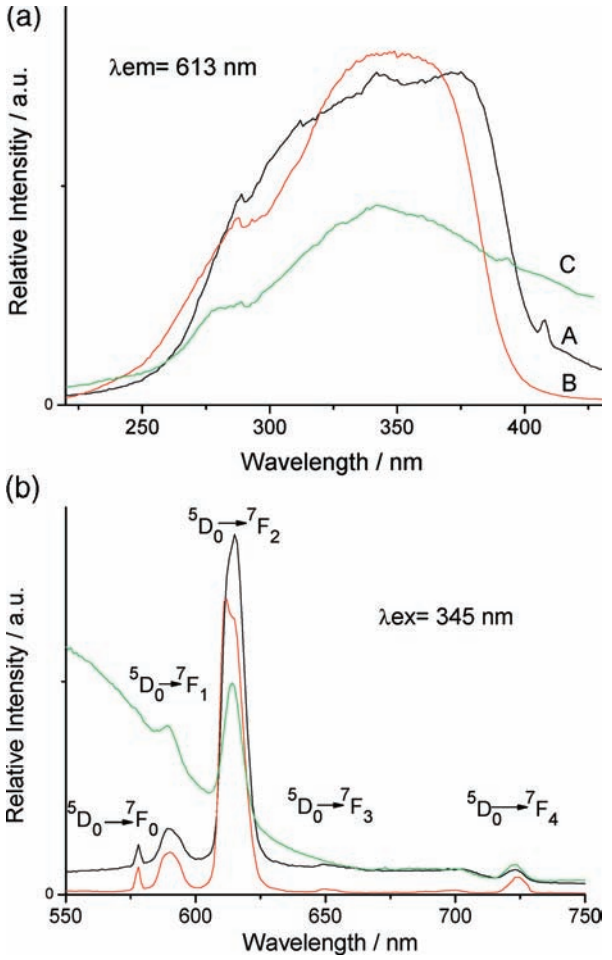

Figure 9. (a) Excitation and (b) emission spectra of the hybrid materials: (A) TTA−Si−Eu−PVPD, (B) TTA−Si−Eu−PMAA, and (C) TTA−Si−Eu−PVPDMAA.

resemblance on the relative fluorescence intensities, stronger than C, and there are two reasonable explanations we presumed. One is that according to Dexter's exchange energy transfer theory[57] and the luminescence theory of lanthanide complexes, the requirement for an efficient intramolecular energy transfer mechanism is that the energy difference between the triplet energy level of the ligand and the resonance energy level of the central Eu^{3+} should be in the range 500−2500 cm^{-1}. Thus, the energy difference ΔE (T_r−Eu^{3+}) between the lowest triplet energy level of TTA (20400 cm^{-1}) and the resonance energy level of Eu^{3+} ($^5D_1$, 19 020 cm^{-1})[61,62] is 1380 cm^{-1}, so that the triplet energy level of TTA is very suitable for the luminescence of Eu^{3+}. It is concluded that the efficient intramolecular energy transfer process in the Eu-TTA system mainly occurred and the energy matching degree between the resonance emissive energy level of Eu^{3+} and the triplet level energy of the polymer precursors PVPD or PMAA are suitable for the intramolecular energy transfer with the existence of β-diketone system, much better than the energy difference between Eu^{3+} and the copolymer precursor PVPDMAA, which shows lower luminescence intensities. The other is that the polymer precursors PVPD and PMAA could successfully be grafted onto the Eu^{3+} and sensitize the luminescence properties of Eu^{3+} with the existence of the β-diketone system, because both the oxygen and nitrogen atoms have a prominent coordination ability with lanthanide ions. Although the precursor PVPDMAA was synthesized through the copolymerization between the 4-vinylpyridine and methacrylic acid, the copolymer PVPDMAA simultaneously has been formed with the enormous chains and the pyridine rings together. When coordinating to rare earth ions, it is difficult for the carboxyl groups and pyridine rings to graft onto Eu^{3+} in such a small space because of the tremendous steric hindrance effect.

3.3.2. Luminescence Decay Times (τ) and Emission Quantum Efficiency (η). According to the emission spectra and the lifetime of the Eu^{3+} first excited level (τ, $^5D_0$), the emission quantum efficiency (η) of the $^5D_0$ excited-state can be determined. Assuming that only nonradiative and radiative processes are essentially involved in the depopulation of the $^5D_0$ excited state, η can be defined as follow:[63]

$$\eta = \frac{A_r}{A_r + A_{nr}} \quad (1)$$

Here, A_r and A_{nr} are radiative and nonradiative transition rates, respectively. A_r can also be obtained by summing over the radiative rates A_{0J} for each $^5D_0 \rightarrow {}^7F_J$ ($J = 0-4$) transitions of Eu^{3+} as follows.

$$A_r = \sum A_{0J} = A_{00} + A_{01} + A_{02} + A_{03} + A_{04} \quad (2)$$

The branching ratio for the $^5D_0 \rightarrow {}^7F_{5,6}$ transitions can be neglected, as they are not detected experimentally. Their influence can be ignored in the depopulation of the $^5D_0$ excited state. Because $^5D_0 \rightarrow {}^7F_1$ belongs to the isolated magnetic dipole transition, it is practically independent of the chemical environments around Eu^{3+} and can be considered as an internal reference for the whole spectra. The experimental coefficients of spontaneous emission A_{0J} can be calculated according to the equation[59,64−66] as follows

$$A_{0J} = A_{01}(I_{0J}/I_{01})(\nu_{01}/\nu_{0J}) \quad (3)$$

Here, A_{0J} is the experimental coefficients of spontaneous emission. A_{01} is the Einstein's coefficient of spontaneous emission between the $^5D_0$ and $^7F_1$ energy levels. In a vacuum, A_{01} could be used as a value of 14.65 s^{-1}, whereas in the air atmosphere, the value of A_{01} can be determined to be ~50 s^{-1} ($A_{01} = n^3 A_{01(vac)}$), [67] when an average index of refraction n equal to 1.506 was considered. I_{01} and I_{0J} are the integrated intensities of the $^5D_0 \rightarrow {}^7F_1$ and $^5D_0 \rightarrow {}^7F_J$ transitions ($J = 0-4$) with ν_{01} and ν_{0J}

(61) Sato, S.; Wada, M. *Bull. Chem. Soc. Jpn.* **1970**, *43*, 1955.
(62) Sager, W. F.; Filipescu, N.; Serafin, F. A. *J. Phys. Chem.* **1965**, *69*, 1092.
(63) Soares-Santos, P. C. R.; Nogueira, H. I. S.; Félix, V.; Drew, M. G. B.; Sa' Ferreira, R. A.; Carlos, L. D.; Trindade, T. *Chem. Mater.* **2003**, *15*, 100.
(64) Teotonio, E. S.; Espínola, J. G. P.; Brito, H. F.; Malta, O. L.; Oliveria, S. F.; de Foria, D. L. A.; Izumi, C. M. S. *Polyhedron.* **2002**, *21*, 1837.
(65) Carlos, L. D.; Messaddeq, Y.; Brito, H. F.; Sa' Ferreira, R. A.; Bermudez, V. D.; Ribeiro, S. J. L. *Adv. Mater.* **2000**, *12*, 594.
(66) Hazenkamp, M. F.; Blasse, G. *Chem. Mater.* **1990**, *2*, 105.
(67) Werts, M. H. V.; Jukes, R. T. F.; Verhoeven, J. W. *Phys. Chem. Chem. Phys.* **2002**, *4*, 1542.

Table 1. Luminescence Quantum Efficiencies and Lifetimes of Solid Hybrid Polymeric Materials

systems	hybrid ploymer TTA−Si−Eu−PVPD	hybrid ploymer TTA−Si−Eu−PMAA	hybrid ploymer TTA−Si−Eu−PVPDMAA
υ_{00} (cm^{-1}) [a]	17301	17301	17274
υ_{01} (cm^{-1}) [a]	16972	16931	16931
υ_{02} (cm^{-1}) [a]	16239	16268	16307
υ_{03} (cm^{-1}) [a]	15396	15396	15403
υ_{04} (cm^{-1}) [a]	13829	13817	13848
I_{00} [b]	28.8	27.4	0
I_{01} [b]	41.0	47.15	91.45
I_{02} [b]	461.1	412.7	209.7
I_{03} [b]	4.2	4.3	1.1
I_{04} [b]	20.1	21.4	22.9
A_{00} (s^{-1})	34.5	29.6	0.0
A_{01} (s^{-1})	50.0	50.0	50.0
A_{02} (s^{-1})	587.3	455.5	126.9
A_{03} (s^{-1})	5.64	5.0	6.8
A_{04} (s^{-1})	30.1	27.8	15.7
τ (μs) [c]	500.3	436.3	405.2
A_{rad} (s^{-1})	707.5	567.9	198.5
τ_{exp}^{-1} (s^{-1})	1999	2292	2468
A_{nrad} (s^{-1})	1292	1724	2269.5
η (%)	35.4	24.8	8.0

[a] The energies of the $^5D_0 \rightarrow {}^7F_J$ transitions (υ_{0J}). [b] The integrated intensity of the $^5D_0 \rightarrow {}^7F_J$ emission peaks. [c] The luminescence decay times of $^5D_0 \rightarrow {}^7F_2$ transitions.

($\upsilon_{0J} = 1/\lambda_J$) energy centers, respectively. υ_{0J} refers to the energy barrier and can be determined with the emission peaks of Eu^{3+}'s $^5D_0 \rightarrow {}^7F_J$ emission transitions. The emission intensity, I, taken as integrated intensity S of the $^5D_0 \rightarrow {}^7F_{0-4}$ emission curves, can be defined as below

$$I_{i-j} = \hbar\omega_{i-j}A_{i-j}N_i \approx S_{i-j} \quad (4)$$

Here, i and j are the initial ($^5D_0$) and final levels ($^7F_{0-4}$), respectively, ω_{i-j} is the transition energy, A_{i-j} is the Einstein's coefficient of spontaneous emission, and N_i is the population of the $^5D_0$ emitting level. On the basis of refs [5, 31, and 68−70], the value of A_{01} is approximately 50 s^{-1} and the lifetime (τ), radiative (A_r), and nonradiative (A_{nr}) transition rates are related through the following equation

$$A_{tot} = 1/\tau = A_r + A_{nr} \quad (5)$$

On the basis of the above discussion, the quantum efficiencies of the three kinds of europium hybrid polymeric materials can be determined as shown in Table 1. Seen from the equation for η, the η value mainly depends on the values of two factors: one is lifetime and the other is the I_{02}/I_{01} ratio. As can be clearly seen from Table 1, the result of quantum efficiencies of the three kinds of the hybrid polymeric materials confirm the conclusion that the polymer and the organic networks have successfully been grafted onto the europium ions through the chemical bonds and the effective intramolecular transfer system has completely achieved in the final products. The quantum efficiencies of TTA−Si−Eu−PVPD (35.4%) and TTA−Si−Eu−PMAA (24.8%) are much higher than that of TTA−Si−Eu−PVPDMAA (8.04%), which can be ascribed to the huge copolymeric structure in such a small unit of the carbon chains with tremendous steric hindrance effect, which could restrict the efficiency of the intramolecular transfer mechanism, or increase nonradiative transition rate and nonradiative multiphonon relaxation aroused by coupling vibrations of hydroxyl groups. The results show that the fluorescence lifetimes of hybrid material TTA−Si−Eu−PVPD are longer than those of TTA−Si−Eu−PMAA because of the possible quenching by hydroxyl or silanol groups in the latter; a the ratio of I_{02}/I_{01} of the former is also larger than that of the latter, so the relative quantum efficiencies of TTA−Si−Eu−PVPD are better (see Table 1), indicating that the hybrid polymer TTA−Si−Eu−PVPD has the more effective red emission and the higher color purity.

4. Conclusion

We have designed and assembled rare earth molecule-based hybrid polymers containing organic carbon chains and organic network (Si−O−Si) and with excellent luminescence properties . The first precursor TTA-Si was constructed by grafting 3-(triethoxysilyl)-propyl isocyanate (TEPIC) onto 2-thenoyltrifluoroacetone (TTA), and the polymer precursors PVPD, PMAA, and PVPDMAA were synthesized through addition polymerization reactions. The hybrid polymers were obtained through coordination, hydrolysis, and condensation. It is illuminated from the analysis of photoluminescence properties and the SEM diagraphs that the three kinds of hybrid materials show the characteristic emission of europium ions and possess monophasic regular microstructure. Furthermore, the hybrid material containing the single-class polymer PVPD presents the most effective intramolecular energy transfer mechanism, bringing the highest fluorescent intensities. Also, the configuration of the polymer could have an important influence on many properties of the hybrid materials because of the tremendous steric hindrance effect. Ulteriorly, these kinds of homogeneous molecular-based hybrid polymeric materials can be expected to have potential and significant applications in optical and electronic devices in the future.

Acknowledgment. This work was supported by the National Natural Science Foundation of China (20671072) and Program for New Century Excellent Talents in University (NCET).

Supporting Information Available: ^{13}C and ^1H NMR spectra (PDF). This material is available free of charge via the Internet at http://pubs.acs.org.

(68) Boyer, J. C.; Vetrone, F.; Capobianco, J. A.; Speghini, A.; Bettinelli, M. *J. Phys. Chem. B.* **2004**, *108*, 20137.
(69) Frey, S. T.; Gong, M. L.; Horrocks, W. D.Jr. *Inorg. Chem.* **1994**, *33*, 3229.
(70) Malta, O. L.; Batista, H. J.; Carlos, L. D. *Chem. Phys.* **2002**, *282*, 21.